Fully coupled CFD/FEA investigations to predict the wave loads on a flexible containership

Lakshmynarayanana, P.A.[1] and Temarel, P.[1]

[1] Fluid Structure Interactions Group, University of Southampton
Southampton, U.K (pl6g12@soton.ac.uk)

ABSTRACT

Increase in computational power has resulted in employing RANS/CFD codes for research and development of marine and offshore units. These applications also include the fluid-structure interactions of large ocean going vessels which require the hydroelastic effects and their associated nonlinearities to be modelled accurately. This paper investigates the symmetric motions and wave-induced loads of a flexible S-175 containership by coupling RANS/CFD and Finite Element software. The numerical predictions of the pitch and vertical bending moment RAOs are compared against experimental measurements and other available numerical predictions. The results indicate that the present two-way coupled method can model with good overall accuracy the nonlinearities associated with the wave bending moments and also predict the 2-node component contribution to good accuracy.

Keywords: Hydroelasticity; Fluid-Structure Interactions; Coupling; RANS/CFD; wave-induced loads; Nonlinearity; Springing

1. INTRODUCTION

Modern seakeeping computations are carried out using a variety of techniques ranging from two- and three-dimensional potential flow methods to three-dimensional (3-D) computations using fully nonlinear unsteady RANS (Reynolds-averaged Navier-Stokes equations) codes (ITTC 2014). The increase in size of ships has resulted in 'softer' hulls which requires the vibratory responses to be included when calculating the wave bending moments (Bishop & Price 1979). The majority of investigations are still carried out using potential flow solvers, with various levels for including nonlinear effects (ISSC. 2012). Although, nonlinear modifications to potential flow solvers have shown to be promising (Park & Temarel 2007), RANS/CFD has the potential to simulate these fluid-structure interactions more realistically, hence, more accurately. Hitherto a few investigations have been carried out using two-way coupling of fluid and structure codes, but mainly to study slamming, whipping and springing (Oberhagemann et al. 2008, Seng et al. 2012 and El Moctar et al. 2017).

In this paper a two-way partitioned coupling between a finite volume CFD method, using Star-CCM+ (version 8.04), and finite element method (FEM), using Abaqus (version 6.13-1), is applied to calculate the wave induced loads of a flexible S-175 containership with a forward velocity in regular head waves. The main emphasis is on the prediction of linear and nonlinear wave loads. The nonlinearities are expressed as the higher order harmonics of the time series signals and high-frequency 2- node springing component. The two-way coupling is applied to investigate the dynamic behavior of the vessel for a range of frequencies and two wave heights. The numerical results are compared to experimental measurements and other numerical predictions showing the suitability of the two-way coupling used to predict the nonlinear effects in relatively severe wave conditions.

* Correspondence to: pl6g12@soton.ac.uk

2. S-175 EXPERIMENTAL MEASUREMENTS

The self-propelled model tests, at Froude number Fn=0.275, used as a primary comparator in this paper were conducted in the towing tank of the China Ship Scientific Research Centre (CSSRC), with tank dimensions of 474m (L) x 14m (B) x 7m (D) (Chen et al. 2001). The elastic model of S-175 was made using ABS plate material ABS702.The main full-scale and model particulars for the S-175 are shown in Table 1. The vertical bending moments were measured at five locations along the model using strain gauges placed on the starboard side-deck plate. In addition to the wave loads, vertical accelerations at the FP, and heave and pitch motions were also measured.

Table 1: Principal particulars of S-175 in full scale and model scale. * are values calculated as per the law of similitude.

Particulars	**Ship**	**Model**
Length (L)	175 m	3.6 m
Draught (T)	9.5 m	0.195 m
Beam (B)	25.4 m	0.523 m
Depth (D)	15.4 m	0.317 m
EI (amidships)	2.28 x 10^{18} kg.mm^2	* 8.4 x10^9 kg.mm^2 10.18 x 10^9 kg.mm^2 (Chen et al 2001)

The following additional experiments are also considered as a benchmark and vast majority of numerical validations utilise them. Watanabe et al. (1989) measured the of effects bow flare on deck wetness and the asymmetry in vertical bending moment on an elastic self-propelled S-175 model, Fn=0.25, built using synthetic resin and foam urethane. To study the influence of different wave heights on the nonlinear characteristics of wave responses, Fonseca & Guedes Soares (2004) tested a model comprising 3 segments connected by springs towed (Fn=0.25) in regular head waves. It should be noted that although the amidships bending stiffness for these two experiments and the computations are according to the scaling of the 2-node natural frequency while the bending stiffness in the experiments by Chen et al (2001) is 20% higher.

3. NUMERICAL METHOD

3.1 Finite Volume Method

The numerical method employed in Star-CCM+ is a finite volume (FV) method in which the flow is assumed to be governed by RANS equations (Ferziger & Peric 2003). The RANS equations reduce to the well-known Euler equations for the case of inviscid flow, used in this paper. Free surface flows are implemented using the Volume of Fluid (VOF) tracking method. The HRIC (High Resolution Interface Capturing) discretization scheme is used for free surface flow along with the VOF tracking in Star-CCM+ (STAR-CCM+ 2012) to maintain a sharp interface. This scheme is a blending of upwind and downwind schemes which is further corrected depending on the local Courant number.

3.2 Finite Element Method

Abaqus is coupled with the Star-CCM+ to solve the structural responses of the flexible containership. It is a displacement-based method where the basis of the finite element solution the principle of virtual work or virtual displacements (Dassault Systèmes 2013).A direct step-by-step

integration is adopted in the present study where the governing equations are integrated over discretised time steps Δt. The temporal integration is performed using a dynamic-implicit scheme which is an extension of the Newmark-β scheme (Dassault Systèmes 2013). The flexibility is modelled using 3-D beam elements (B31). Presently, a structure modelled using beam elements cannot be directly coupled with the fluid model in Star-CCM+. Hence, membrane elements (SFM3D4) are used to represent the wetted surface area and are connected to the beam nodes.

3.3 Co-Simulation

To solve the FSI problem with the flexible S-175, the fluid and structural solvers run in a coupled manner. A partitioned algorithm is used to execute the two-way coupling or co-simulation where separate solvers for fluid (Star-CCM+) and structure (Abaqus) are employed. The information is exchanged between them at the interface (S-175 hull) sequentially and solved iteratively. The coupling is performed by exchanging pressure and nodal displacements, known as field data, between Star-CCM+ and Abaqus, respectively. The structural deformations of the S-175 model, due to the applied fluid pressures, are fed back into the fluid solver to redefine the body and the fluid grid. In the present study, a two-way implicit coupling method is used to simulate the hydroelastic response of S-175 containership. In an implicit coupling, the information is exchanged between the software more than once every time step to simulate the variation in hydrodynamic loading and structural velocities. The number of such exchanges per time step is critical for the stability and accuracy of the coupled simulations (Camilleri et al. 2015).

Finite volume codes store the scalar quantities at each cell center or the face centroid of the mesh and finite element codes store the solution at the vertices of the mesh. The fluid pressures at the interface stored at the face centroid of the CVs are mapped on the face centres of the SFM3D4 membrane (surface) elements using least square interpolation. When the nodal displacements are mapped from a finite element mesh to a finite volume mesh a shape function interpolation is used.

3.4 Grid adaptation method

Grid adaptation, as a consequence of the motion and deformation of the body at the free surface, is implemented using two different methods, namely ‘morphing’/deforming mesh and ‘overset’ grids. The deformation of the body is carried out using ‘morphing’. The nodal displacements imported from Abaqus are used to redistribute the mesh vertices by generating an interpolation field throughout the fluid domain. Morphing could, however, create problems in the case of a body undergoing large motions in waves. The deformation of the entire grid could result in the free surface falling outside the refined region of the grid; additionally, the quality of the cells deformed can become poor resulting in numerical errors. To avoid this problem, an overset grid is used. An area around the body is defined as overset boundary (see Figure 1). The overset boundaries are attached to the floating body and move with it freely, with the resultant motion in waves. The motion of the overset grid is relative to the fixed background region that encompasses the fluid domain.

A combination of overset mesh and mesh morphing is used in the case of the coupled simulations. The nodal displacements from Abaqus, which includes both the rigid body motion and the distortions, cause a deformation of the body by generating an interpolation field as mentioned above. The overset boundaries then move in response to the interpolation field created by the mesh morpher which in turn helps to maintain good quality cells in the region.

4. NUMERICAL SETUP

4.1 Computational Domain and Meshing strategy

The coordinate system of the computational domain is defined such that the longitudinal direction of the model is aligned with the x-axis with the stern located at x=0 and the side wall extended along

the y-axis. The extension of the computational domain in all directions is shown in Figure 1. Since the problem is symmetric with respect to the y-axis the coupled analyses were carried out on one-half of the solution domain. A constant damping distance of 2.0 L is set for all incident wave lengths investigated. A trimmed Cartesian grid is used for the discretising the 3-D domain. The ensuing mesh was made up effectively of unstructured hexahedral cells with cells trimmed adjacent to the ship model. Furthermore, the outlet and the side-wall boundaries are extruded using user specified stretching parameters.

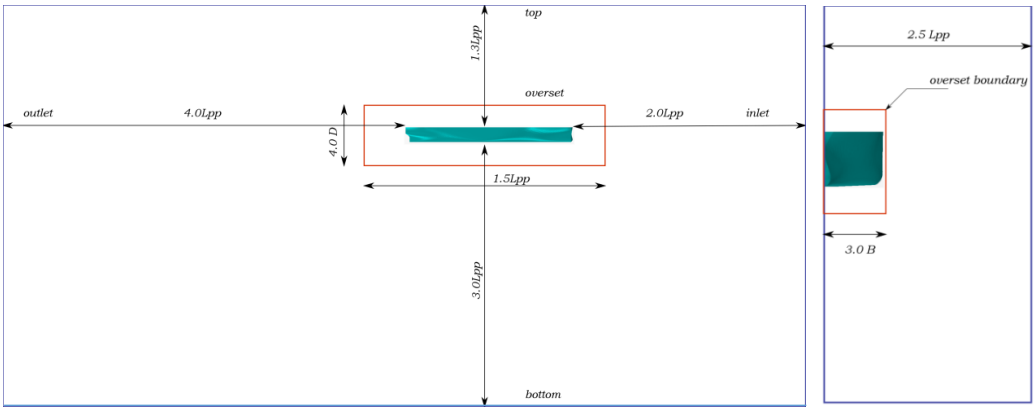

Figure 1: The 3-D extension of the CFD domain in Star-CCM+.

Taking into consideration the number of test cases that needs to be simulated, it was decided to carry out the computations on one single mesh for each wave height, suitable for the range of wave frequencies investigated. Firstly, the grid size on the free surface is set for λ/L=1.0. Following recommendations by STAR-CCM+ (2012) and (ITTC 2011), 80 cells per wave length are used. It should be noted that the experience obtained from the barge co-simulations (Lakshmynarayanana et al. 2015) indicate that a minimum of 40 cells per wave length and 20 cells per wave height is sufficient to produce a stable wave with acceptable dissipation. Using the mesh created for λ/L=1.0 for other wavelengths, 50 and 160 cells are contained per wave length for λ/L=0.6 and λ/L=2.0, respectively. Approximately 22 cells are contained per wave height in the free surface region for both wave heights investigated, namely L/30 and L/50, which is in line with ITTC (2011) recommendations.

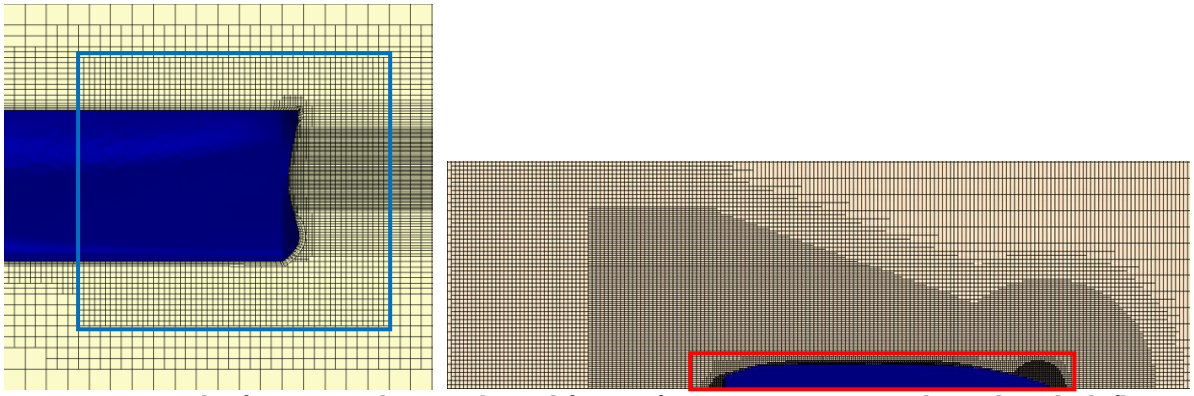

Figure 2: Grid refinement in bow, wake and free surface region to capture the violent deck flows; λ/L =1, H/L=50.

Thereafter the refinements adjacent to the hull and in the wake region were set to adequately capture the severe free surface flows arising due to the green water effects and the wake field of the advancing ship. Kim & Lee (2011) suggest a minimum of 150 grid cells per wave length near the hull surface in both upstream and downstream directions when severe motions inducing slamming and green water effects are present. In the co-simulations, for λ/L =1, 160 cells per wave length (shown by the red box in Figure **2**) are placed in the vicinity of the hull. Using this near hull refinement results in

approximately 100 and 320 cells per wave length for λ/L=0.6 and λ/L=2.0, respectively. In addition the bow (shown by the blue box in Figure 2) and stern regions contain 50 grid point refinement along the depth. The total cell count of the fluid domain is approximately 3.5 million.

4.2 FE model

The structural properties for the FE beam model were calculated using scaling laws from the full scale mass and structural properties published by Wu & Hermundstad (2002). The structural model consists of 100 3-D quadratic Timoshenko beam elements, B31. The material properties of the beam elements are defined as that of Aluminium, corresponding to the flexible backbone of the model. The effective shear area was available (Wu & Hermundstad, 2002) and was taken into account in the F E model.

The beam is shown in red colour in the FE model assembly shown in Figure 3. The hull is cut arbitrarily to illustrate the FE model details, with the beam positioned at a height corresponding to the VCG of the S-175.

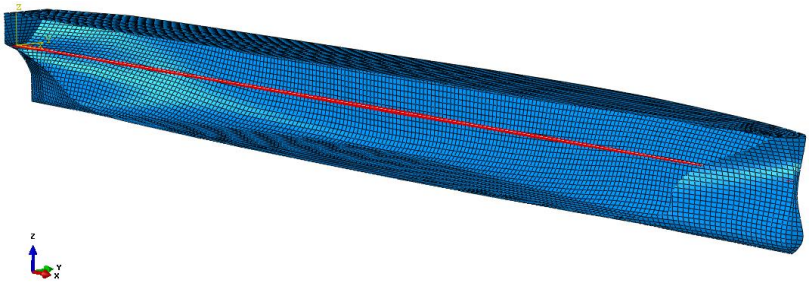

Figure 3: S-175 FE model. The red line represents the beam model.

The FE model is constrained for y-axis (no sway) translations and rotations about the x and z-axes (no roll and yaw). The forward velocity of the S-175 containership in the coupled analyses is simulated by assigning an additional velocity of propagation, equal to the model velocity, to the regular wave. An additional constraint of zero translation in the x direction to a beam node close to the LCG of the model is defined to restrict the longitudinal drift.

5. RESULTS AND DISCUSSION

5.1 Dry Natural frequencies

The first two dry natural frequencies of the model, evaluated using Block Laconzs eigen value extraction method, are shown in Table **2**, together with those obtained by finite difference method (Bishop et al. (1977) including the effects of effective shear area. There is good agreement between the FE models and the 2-D finite difference results. It should be noted that the 2-node dry hull natural frequency of the model by Chen et al. (2010) is 12.27 Hz.

Table 2: Dry natural frequencies (Hz) of the S-175 model – in brackets (rad/s).

Mode	**Abaqus**	**Finite difference**
2-node	11.12 (69.92)	10.90 (68.493)
3-node	25.22 (158.49)	24.31 (152.76)

5.2 Motions in waves

For numerical validation, Chen et al. (2001) is treated as the primary comparator, namely the current numerical predictions are for Fn=0.275. It was not possible to exactly replicate the experimental conditions, for example, the numerical model is closer to a towed model than a self-propelled model. The 2-D linear predictions are obtained using the 2-D hydroelasticity method (Bishop & Price 1979) with 20 strips and Lewis conformal mapping.

In the numerical analysis and in the experiment, the incoming wave is monitored at one ship length (3.6m) in front of the model. The wave heights obtained from the simulations were calculated as the average of peak-to-trough for ten complete cycles. The incoming wave was stable in the simulations and the decrease in amplitude is less than 7% for the wave frequencies investigated. Heave, Pitch and the vertical accelerations were calculated from the coupled simulations, however, only the pitch responses are shown in this paper. The pitch responses are plotted against the non-dimensionalised wave frequency $\omega\sqrt{(L/g)}$, where ω is the incident wave frequency.

The pitch RAOs predicted, shown in Figure 4, displays good agreement with the experiments except in the non-dimensional frequency range of 2.0~2.2 where it is over predicted. The magnitude of pitch angle is very small for this model in the range of 0.6~4.0 degrees. The predictions in this region ($\omega\sqrt{(L/g)}$ 2.0~2.2) are closer to the measurements conducted by Fonseca & Guedes Soares (2004b). The CFD/FEA pitch RAO decreases by about 15% with the increase in wave height. The measurements by Chen et al. (2001) exhibit a sharp decrease in the non-dimensionalised frequency region 2.0~2.2; not noted by other experimentalists. Chen et al (2001) do not offer any specific reasoning about this odd behaviour. It should also be noted that the 2-D linear (hydroelasticity) pitch RAO predictions agree reasonably well with the CFD predictions.

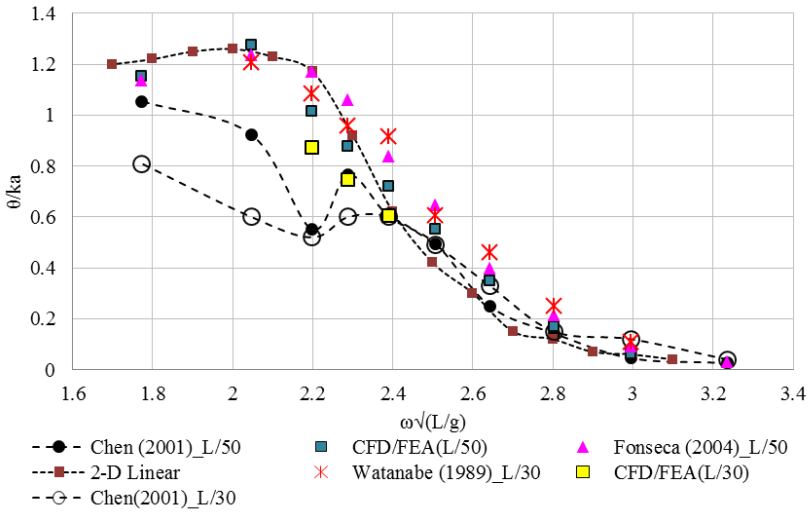

Figure 4: RAO of pitch (θ) from the coupled simulations along with 2-D and experimental measurements; k: wave number, a: wave amplitude.

5.3 Symmetric Bending moment in waves

The first harmonic of amidships wave bending moment estimated using the coupling method is compared with 2-D linear, experimental measurements and with the nonlinear strip theory results by Wu & Hermundstad (2002). The 2-D linear predictions are obtained using the 2-D hydroelasticity method (Bishop & Price 1979) with 20 strips, Lewis conformal mapping and Timoshenko beam idealisation; the structural damping has been set to zero. Comparing the predictions for H/L=50 in Figure 5, the agreement between the two methods (i.e. 2-D linear and CFD/FEA) is seemingly good in the region of λ/L =0.6~0.9. In the range of λ/L =1.0~2.0 the 2-D linear, as well as the nonlinear strip theory predictions are larger. The difference between the 1st harmonic of VBM approaches a maximum of about 18-20% in the region of non-dim frequency 1.5~2.0. The bending moments

predicted by the 2-way coupling in this region is under-predicted when compared to 2-D linear and even the experiments. In relatively shorter wave length, i.e. λ/L =0.6~0.9, the agreement between the two-way coupling and the other two numerical methods is excellent, but not so with the experiments.

For H=L/50 the amidships bending moment comparisons between the present method and the experiment amidships produce small differences in the resonant (ship-wave matching) region; however, there is over prediction in the shorter waves by a maximum of about 35% and under prediction by the same amount in the longer waves. The cause for this under prediction is undetermined. The correspondence between the two-way coupling and the three experiments is excellent in the region of λ/L= 1.0~1.3. Some differences can also be noted between the different experiments but these are under 15%. Increase in wave height causes an increase in the amidship bending moment by 10% in the coupled simulations. A definite peak is noted in Chen et al. (2001) at λ/L = 1.2 and the measurement is 15% greater than the simulations and the other experiment.

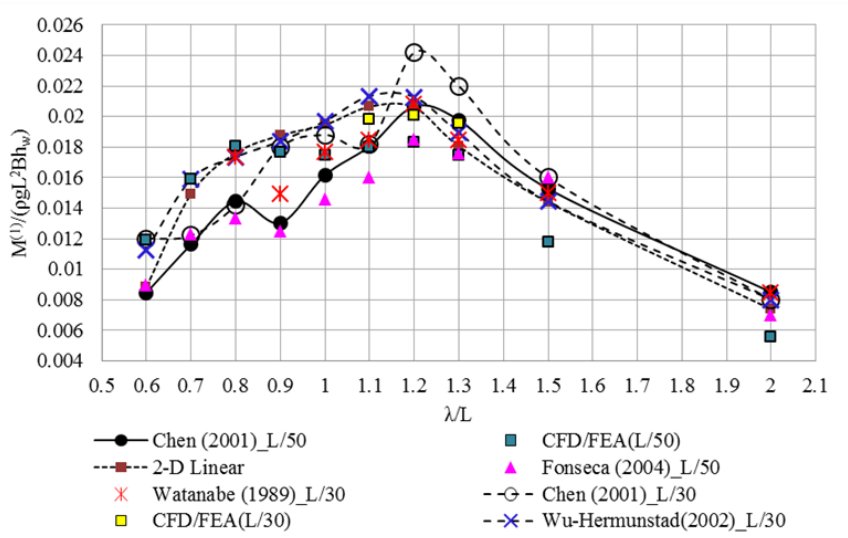

Figure 5: Non-dimensional amplitude of first harmonic of VBM amidships.

A comparative study using various established partially non-linear methods and the model tests of S-175 was undertaken by ISSC (2000). The codes were fundamentally modifications of linear strip theory to account for non-linear effects in various ways. The majority of the methods over-predict the amidships bending moment in the region of λ/L 0.7~1.2. Apart from the inevitable uncertainties in measurements, it can be definitely stated that the co-simuation is capable of predicting the linear wave loads to a similar degree of accuracy, if not better. Another salient feature from the plots is that the 2-D linear prediction, which is the most efficient of all methods, is able to give a good estimation of the first harmonic bending moment when compared to other methods of varying complexity.

5.4 Nonlinear effects in wave loads

The 2nd harmonic of bending moment amidships calculated using CFD/FEA and measured from experiments are shown in Figure 6. The numerical predictions at amidships have maximum values that vary between 15% and 30% of the first-harmonic amplitudes, whereas in the experiments by Chen et al. (2001) it varies between 2%-10% of the first harmonic. The numerical predictions estimate higher second harmonics (λ/L=1~1.5) compared to Chen et al. (2001), but produce good agreement with the measurements by Watanabe et al. (1989), the latter for slightly lower speed. In steep waves, the aforementioned two experiments record large differences, considering the fact that an elastic self-propelled model is used in both. With increase in wave height the predicted second harmonics get stronger in the numerical predictions to about 11-30% of the first harmonic in the range of λ/L=1.1~1.3.

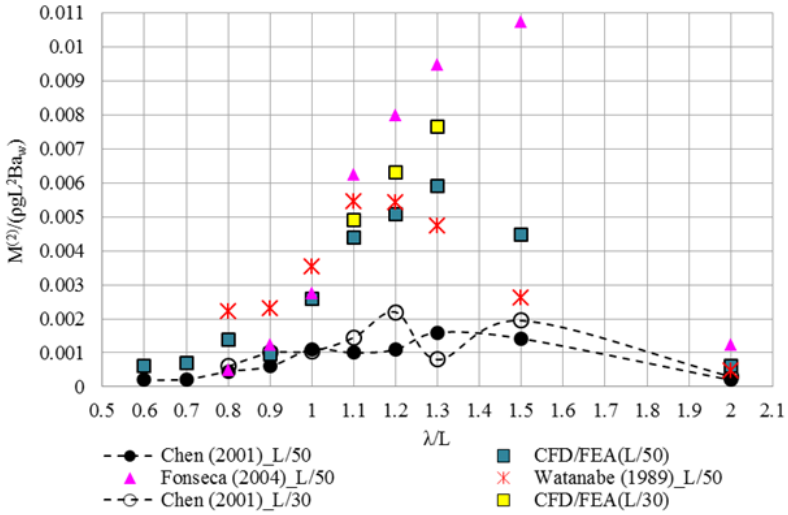

Figure 6: Non-dimensional amplitudes of 2nd harmonic of VBM amidships.

The third harmonics of vertical bending moment at amidships is shown in Figure 7. Once again the CFD/FEA tends to overestimate the nonlinear effects, by about twice, in the region of λ/L=1.1~1.3; nevertheless, the comparison is better than the second harmonic predictions when Chen et al (2001) is considered. In general, a good agreement is achieved in the case of the third harmonics. The numerical predictions reveal that the third harmonics are of the order of 5-10% of the first harmonics. It is noteworthy that the two-way coupled method is able to capture even the relatively weaker nonlinear effects in the wave loads to acceptable level of accuracy. This would mean that, in cases where the nonlinear effects could be stronger, the coupled method could be used to make estimations with good engineering accuracy.

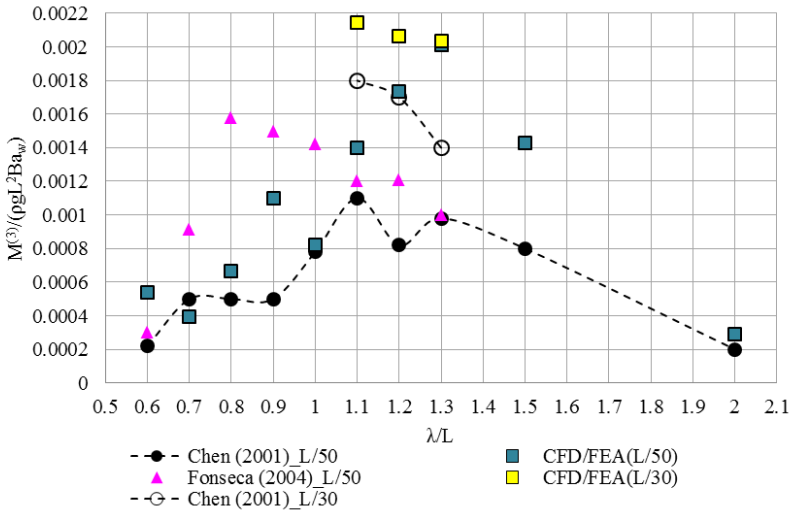

Figure 7: Non-dimensional amplitudes of 3rd harmonic of VBM amidships

The 2-node mode contribution of the vertical bending moment amidships is shown in Figure 8. It should be noted that the 2-node wet resonance frequency is 8.88 Hz. The numerical predictions agree well at some wave frequencies, although there is substantial deviation at certain frequencies. The order of magnitude of the 2-node component is similar to the experiments, except at λ/L=1.0 and 1.2. The predictions show an anomaly at λ/L=1.0 and 1.2 and the predicted response is larger by nearly 6 times that of the measurements. The presence of higher frequency components was clearly identifiable in the time histories of bending moments. The predictions for H=L/30 is good when compared to experimental measurements for the three wave lengths investigated. It should be noted that the 2-node wet resonance (encounter) frequency corresponds to the 8th and 9th harmonic,

respectively, of the encounter frequencies for λ/L=1.0 and 1.2. The importance of this will become apparent in the next section.

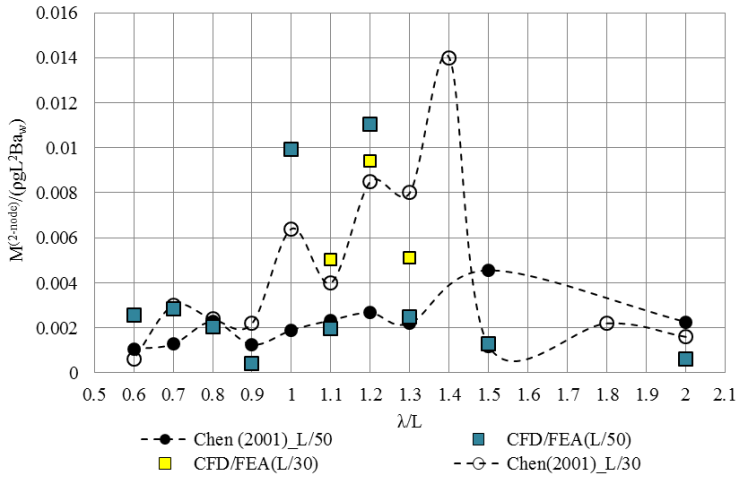

Figure 8: 2-node component in VBM amidships

5.5 Effect of structural damping on wave loads

Wu et al. (2003) estimated the 2-node damping ratio of S-175 model in still water from the time history of amidships impulse-exciting responses to be 0.067. This damping ratio is a combination of hydrodynamic and structural damping. In this case the structural damping is estimated approximately as 1% of critical damping. This value is calculated from the case studies of ships in Bishop& Price (1979) which gives an approximate structural damping vs hydrodynamic damping comparison. Rayleigh's damping is used to assign structural damping to the beam model using only the mass proportional damping ratio α.

The wave loads are recalculated using structural damping for λ/L=1.0~1.3. The numerical predictions of the first and higher harmonic contributions and the 2- node component is shown in Figure 9. Ideally, the structural damping in the numerical model should not have any effect on the first harmonic of the VBM. Figure 9 also shows only a marginal variation in the first harmonic of the amidships bending moment. Regarding the higher order harmonics, the numerical predictions, by and large, either move closer towards the experiments by Chen et al (2001) or exhibit negligible change.

There is an overwhelming change in the 2-node flexible mode component in the aforementioned frequencies and decreases by about 60-70% compared to the undamped case. The agreement is excellent when compared with measurements. There is some influence of the structural damping on the higher order harmonics but the effect is much stronger in the 2-node component. Only four frequencies were investigated with one damping coefficient. The coupled method is capable of capturing the 2-node contribution to a good degree of accuracy when compared to the experiments.

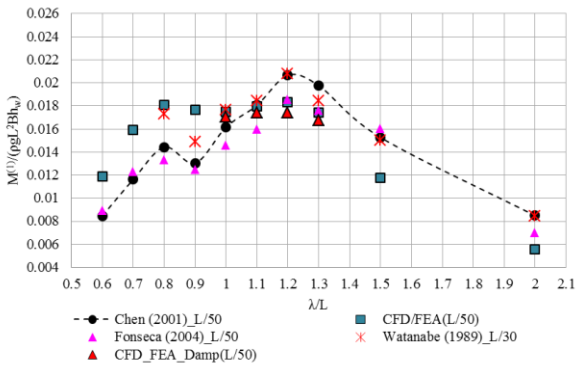

(a)

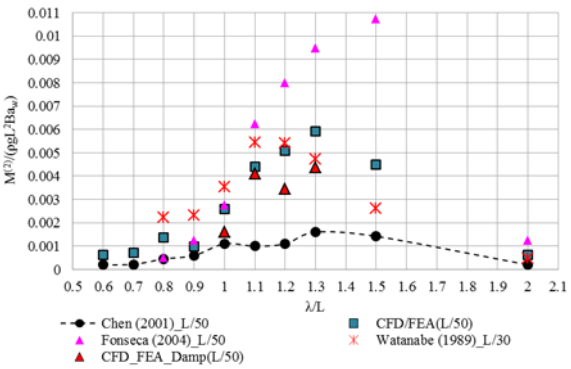

(b)

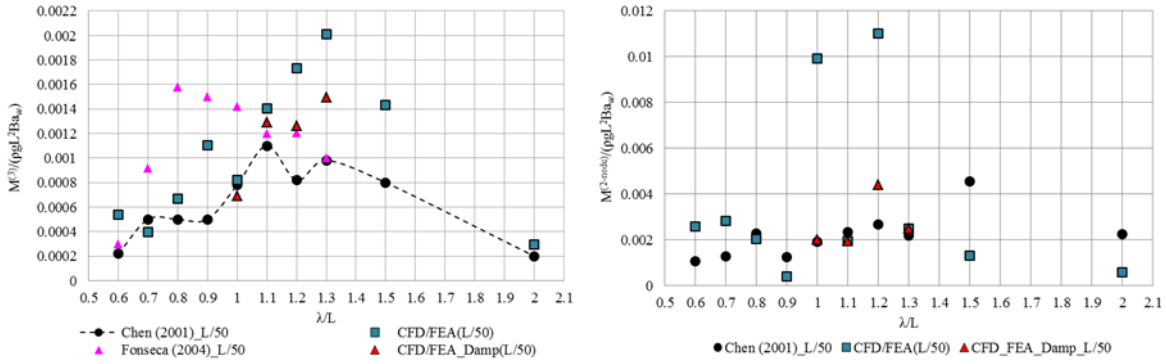

(c) (d)

Figure 9: Non-dimensional amplitudes of (a) 1st harmonic of VBM (b) 2nd harmonic (c) 3rd harmonic (d) 2-node component amidships with and without structural damping

6. CONCLUSIONS

A flexible S-175 containership model with forward speed is used to validate the (inviscid) CFD/FEA co-simulation by comparing the wave-induced load predictions with experimental measurements of Chen et al. (2001) and others, as well as 2-D linear hydroelasticity.

The nonlinearity in wave loads is reflected in the higher order harmonics of the wave encounter frequency and the 2-node flexible wet resonance frequency. The first harmonic of vertical bending moment (VBM) amidships predicted around the resonance region (ship-wave matching region) agrees well with measurements. In the longer waves, the first harmonic VBM amidships was under predicted by about 30-35% when compared with measurements and 2-D linear hydroelasticity.

The present method predicts stronger second and third harmonic components when compared with Chen et al. (2001), but agrees well with Watanabe et al. (1989). The nonlinear loads measured by various experiments also showed more scatter than the first harmonic VBM. The 2-node flexible mode contribution of the VBM amidships predicted using the co-simulation showed the importance of including the effects of structural damping in the numerical model. Furthermore, the inclusion of structural damping had negligible to small influence on the first, second and third harmonics.

This methodology might be neglecting certain key fundamentals of CFD investigations, such as grid independence, but has proved to be numerically efficient and capable of producing results with good engineering accuracy, a testament to the creativity process of mesh design. Nevertheless, the drawback of the CFD/FEA method is the computational time required to carry out these predictions which makes the 2-D linear methods more efficient for the first harmonic wave loads.

Future work should focus on (i) reducing the size of the mesh and its consequent effects on predicted linear and nonlinear VBM, (ii) preforming co-simulation in long- and short-crested irregular waves with focus on whipping, springing and their influence on fatigue life and (iii) performing co-simulation that also includes coupled antisymmetric horizontal-bending and twisting. Finally, this co-simulation provides the opportunity to investigate the influence of diffracted and radiated waves on nonlinear springing.

ACKNOWLEDGEMENTS

The authors acknowledge the support of the Lloyd's Register Foundation through its University of Southampton Technology Centre and Lloyd's Register.

REFERENCES

Bishop, R.E.D. & Price, W.G., 1979. *Hydroelasticiy of Ships*, Cambridge University Press.

Bishop, R.E.D., Price, W.G. & Tam, P.K.Y., 1977. A unified dynamic analysis of ship response to waves. *Trans. R. Inst Nav. Architects*, 119, pp.363–390.

Camilleri, J., Temarel, P. & Taunton, D., 2015. Two-dimensional numerical modelling of slamming impact loads on high-speed craft. In *7th International Conference on HYEL*. Split, Croatia, pp. 43–54.

Chen, R.Z., Du, S.X., Wu, Y.S., Lin, J.R., Hu, J.J. & Yue, Y.L., 2001. Experiment on extreme wave loads of a flexible ship model. In *PRADS*. pp. 871–878.

Dassault Systèmes, 2013. *Abaqus 6.13-1 Manual*, Providence, RI, USA.

Ferziger, J.. & Peric, M., 2003. *Computational Methods for Fluid Dynamics* 3rd Editio., Springer, Berlin.

Fonseca, N. & Guedes Soares, C., 2004. Experimental Investigation of the Nonlinear Effects on the Vertical Motions and Loads of a Containership in Regular Waves. *J. Ship Res.*, 48(2), pp.118–147.

ISSC., 2000. Committee VI.1. Extreme Hull Girder Loading. *Proceedings of the 14th International Ship and Offshore Structures Congress 2000, Vol. 2 (Eds. Ohtsubo, H. and Sumi, Y.)*, pp.263–320.

ISSC., 2012. Report of Committee I.2: Loads. In Proceedings of the 18th International Ship and Offshore Structures Congress, Rostock, Germany. , 1, pp.79–150.

ITTC, 2011. Practical Guidelines for Ship CFD Applications. In *International Towing Tank Conference*. pp. 1–18. Available at: https://ittc.info/media/1357/75-03-02-03.pdf.

ITTC, 2014. The Seakeeping Committe final report and recommendations. In the Proceedings of 26th ITTC, Copenhagen.

Kim, S.P. & Lee, H., 2011. Fully nonlinear seakeeping analysis based on CFD simualtions. In *In Proceedings of the 21st International Offshore and Polar Engineering Conference*. Hawaii, U.S.A, pp. 970–974.

Lakshmynarayanana, P., Temarel, P. & Chen, Z., 2015. Coupled Fluid-Structure Interaction to model Three-Dimensional Dynamic Behaviour of Ship in Waves. In *7th International Conference on HYEL*. pp. 623–637.

El Moctar, O., Ley, J., Oberhagemann, J. & Schellin, T., 2017. Nonlinear computational methods for hydroelastic effects of ships in extreme seas. *Ocean Engineering*, 130, pp.659–673.

Park, J.H. & Temarel, P., 2007. The Influence of Nonlinearities on Wave-induced Motions and Loads Predicted by Two-dimensional Hydroelasticity Analysis. *In Proceeding of the 10th International Symposium on Practical Design of Ships and Other Floating Structures,Houston, Texas*, 1, pp.27–34.

Seng, S., Andersen, I.M. V & Jensen, J.J., 2012. On the influence of hull girder flexibility on the wave induce bending moments. In *6th International Conference on Hydroelasticity in Marine Technology*.

STAR-CCM+, 2012. STAR-CCM+ version 8.04 manual.

Watanabe, I., Keno, M. & Sawada, H., 1989. Effects of bow flare shape on wave loads of a container ship. *Journal of the Society of Naval Architects of Japan*, 166, pp.259–299.

Wu, M. & Hermundstad, O.A., 2002. Time-domain simulation of wave-induced nonlinear motions and loads and its applications in ship design. *Marine Structures*, 15(6), pp.561–597.